cmgh
CELLULAR AND MOLECULAR GASTROENTEROLOGY AND HEPATOLOGY

ORIGINAL RESEARCH

Androgen Signaling in ILC2s Drives Sex Differences in *Helicobacter*-induced Gastric Inflammation and Atrophy

Benjamin C. Duncan, Maeve T. Morris, Jordan L. Pascoe, Stuti Khadka, Lei Wang, Gangqing Hu, and Jonathan T. Busada

Department of Microbiology, Immunology and Cell Biology, West Virginia University School of Medicine, Morgantown, West Virginia

Androgens Modulate ILC2-Regulated Immune Networks During *Helicobacter*-Infection

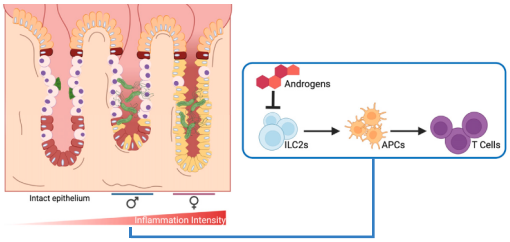

Androgen signaling modulates ILC2 activation which suppresses downstream immune crosstalk, thereby reducing gastric epithelial damage and maintaining epithelial integrity during *Helicobacter* infections. In the absence of androgen signaling, heightened ILC2–APC–T cell interactions promote increased inflammatory intensity, gastric atrophy and metaplasia development.

SUMMARY

During *Helicobacter* infection, androgens inhibit type two innate lymphoid cell (ILC2) activation, thereby reducing gastric inflammation and atrophy in males. In females, the lack of androgen signaling enhances ILC2-driven immune responses, promoting epithelial atrophy and metaplasia, and revealing a key mechanism underlying sex differences in gastric disease susceptibility.

BACKGROUND & AIMS: Gastric cancer is the fifth most common cancer worldwide. Men are disproportionately affected by gastric cancer, which ranks as the fourth most common cancer in men compared with eighth in women. Chronic inflammation driven by *Helicobacter pylori* infection remains the leading gastric cancer risk factor. Evidence suggests that sex hormones shape sex differences in infection outcomes and cancer susceptibility. This study investigates how androgens influence the gastric inflammatory response to *Helicobacter* infection and contribute to sex disparities in pre-dysplastic disease progression.

METHODS: Male and female mice were colonized with *Helicobacter felis*. Androgen levels were manipulated by bilateral castration in males and dihydrotestosterone (DHT) treatment in females. Single-cell RNA sequencing was used to identify androgen-responsive leukocyte populations and to establish cell communication networks between leukocyte clusters. The functional roles of these cells were further defined using type 2 innate lymphoid cell (ILC2)- and T cell-deficient mouse models.

RESULTS: Infected female mice developed significantly more severe gastric inflammation, atrophy, and metaplasia infection compared with males. Androgen depletion by castration increased gastric inflammation and accelerated preneoplastic lesion development, whereas these pathological features were reduced by DHT treatment. Androgen-responsive ILC2s were key initiators of gastric inflammation, and ILC2 depletion abolished the sex differences in *H felis* pathogenesis.

CONCLUSIONS: This study reveals that androgens protect from *Helicobacter*-induced gastric inflammation by modulating ILC2 activation. These findings indicate that ILC2s serve as master regulators of *Helicobacter*-driven gastric inflammation and highlight their role in directing sex differences in the progression of pre-dysplastic disease. *(Cell Mol Gastroenterol Hepatol 2026;20:101690; https://doi.org/10.1016/j.jcmgh.2025.101690)*

Keywords: Gastric Cancer; *Helicobacter pylori*; Pyloric Metaplasia; Sex Differences; Testosterone.

Males and females exhibit pronounced sexual dimorphism in susceptibility to infectious disease, immunological disorders, and cancer. Females tend to mount more robust inflammatory responses to infections and vaccinations as well as stronger anti-tumor immune responses. However, this heightened immune reactivity also contributes to their significantly higher incidence of autoimmune diseases.[1–3] In contrast, males typically exhibit weaker immune responses, leading to increased susceptibility to infections and malignancies. Although a combination of genetic, hormonal, and behavioral factors underlies these sex differences, sex hormones play a central role in shaping immune function. Although their effects on the immune system are pleiotropic, estrogens tend to enhance immune function by promoting effector T cell responses and stimulating cytokine production.[1] In contrast, androgens are predominantly anti-inflammatory, suppressing both innate and adaptive immune responses and inhibiting the transcription of genes encoding proinflammatory cytokines.[2] These immunosuppressive effects of androgens are thought to contribute to the higher rates of infection and cancer observed in males.

Gastric cancer is the fifth most common cancer worldwide.[4] Infection by the Gram-negative bacteria *Helicobacter pylori* remains the leading gastric cancer risk factor and is associated with up to 90% of non-cardia gastric cancer cases.[5] Chronic inflammation is a critical driver of *H pylori* pathogenesis and strong Th1/Th17-polarized immune responses drive parietal cell atrophy and are associated with increased gastric cancer risk.[6–9] In contrast, although tolerogenic immune responses protect by limiting overt gastric atrophy, Th2-associated cytokines are reported to drive metaplasia maturation and may favor dysplasia development.[10–12] In experimental models, chronic gastric inflammation through overexpression of proinflammatory cytokines such as interleukin (IL)1B or disruption of the immune regulators such as NF-κB1 drive spontaneous dysplastic lesion formation, even in the absence of *H pylori* infection.[13,14] Thus, inflammation is both necessary and sufficient to drive gastric carcinogenesis. Perplexingly, despite the link between intense immune responses and gastric carcinogenesis, gastric cancer is a male-biased disease, with more than 65% of global gastric cancer cases diagnosed in men.[4] Although lifestyle factors such as smoking and alcohol consumption contribute to male susceptibility, sex disparity persists even after adjusting for these risks,[15,16] suggesting that endogenous biological factors—such as sex hormones—influence gastric cancer risk. However, little is known about how sex impacts the gastric inflammatory response to *H pylori* infection.

Type 2 innate lymphoid cells (ILC2s) are tissue-resident leukocytes in the gastric mucosa. Upon epithelial damage, ILC2s respond by stimulating gastric macrophage recruitment and producing IL13, promoting pyloric metaplasia (PM) maturation.[11,12,17–19] Although ILC2s were initially described for their role in producing group 2 cytokines such as IL5 and IL13 in response to damage-associated molecular patterns (DAMPS), they are now recognized as highly plastic, and capable of producing mixed Th1/Th2-associated cytokines during bacterial infections.[20,21] We have previously demonstrated that androgens suppress gastric ILC2 function by regulating the transcription of proinflammatory cytokines, such as *Il13* and *Csf2*.[17] Similar findings have been made in the pulmonary system, where androgen suppression of ILC2s protects from hypersensitivity reactions.[22,23] Recently, ILC2s were also shown to control sex differences in the skin in response to *Staph epidermidis* infection, directing antigen-presenting cell (APC) and T cell recruitment and activation.[24] In the stomach, *H pylori* infection increases the number of ILC2s, where they contribute to humoral immune responses.[25] However, their role in *H pylori*-associated atrophic gastritis and subsequent metaplasia remains unclear.

We previously showed that androgens control sex differences in gastric inflammation and protect males from metaplasia initiation.[17] Here, we utilize *Helicobacter felis* to model the intense T cell responses stimulated by *H pylori* infection in humans that drives gastric inflammation and subsequent preneoplastic lesion development. *H felis* infection elicits strong gastric T cell responses that closely mimic the inflammatory reaction seen with *H pylori* in humans.[26,27] By contrast, *H pylori* infection in mice triggers relatively weak T cell responses and requires a longer time to drive gastric atrophy and metaplasia. Our findings reveal that males are significantly protected from *Helicobacter*-associated pathologies. We identified a novel ILC2-APC-T cell axis that controls sex differences in *H felis*-induced gastric inflammation. Moreover, we provide evidence that androgens suppress gastric inflammation, as androgen depletion by castration significantly increased inflammation and accelerated preneoplastic lesion development in males. Collectively, our results demonstrate a critical role for ILC2s in shaping sex differences in the gastric response to *Helicobacter* infection.

Abbreviations used in this paper: **ANOVA, analysis of variance; APC, antigen-presenting cell; AR, androgen receptor; CFU, colony-forming units; DAMP, damage-associated molecular pattern; DAPI, 4′,6-diamidino-2-phenylindole; DEG, differentially expressed gene; DHT, dihydrotestosterone; FBS, fetal bovine serum; GI, gastrointestinal; GM-CSF, granulocyte-macrophage colony-stimulating factor; GSEA, Gene Set Enrichment Analysis; GSII, Griffonia simplicifolia lectin; H&E, hematoxylin and eosin; HBSS, Hanks' Balanced Salt Solution; IL, interleukin; ILC2, type 2 innate lymphoid cell; ILC2-DTx, type 2 innate lymphoid cell diphtheria toxin depletion; Int, intact; KEGG, Kyoto Encyclopedia of Genes and Genomes; logFC, log2 fold change; NES, normalized enrichment score; NK, natural killer; PBS, phosphate buffered saline; PM, pyloric metaplasia; qRT-PCR, quantitative reverse transcription polymerase chain reaction; RNA-seq, RNA sequencing; RPKM, reads per kilobase per million; scRNA, single-cell RNA; SD, standard deviation; TCR, T cell receptor; TCR$\beta\delta$ KO, T cell receptor beta/delta knockout; UMAP, Uniform Manifold Approximation and Projection; WT, wild-type.**

Most current article

© 2025 The Authors. Published by Elsevier Inc. on behalf of the AGA Institute. This is an open access article under the CC BY-NC-ND license (http://creativecommons.org/licenses/by-nc-nd/4.0/).

2352-345X
https://doi.org/10.1016/j.jcmgh.2025.101690

Results

Males Mount Blunted Inflammatory Responses to Helicobacter *Infection Compared With Females*

Chronic inflammation is a key driver of *H pylori* pathophysiology, promoting gastric atrophy and metaplasia development and shaping gastric cancer risk.[28] Females tend to mount more robust inflammatory responses to infection compared with males.[1] To investigate sex differences in *Helicobacter*-induced gastric inflammation, we utilized the well-established *Helicobacter felis* model, which rapidly induces gastric inflammation, atrophy, and metaplasia in mice.[26] Male and female C57BL/6J mice were colonized by *H felis,* and the stomachs were collected 2 months post-colonization. Evaluation by CD45 immunostaining and flow cytometry indicated that male and female mock-infected mice did not exhibit significant sex differences in gastric-resident immune cells (Figure 1*A*–*B*). *H felis* colonization significantly increased leukocyte infiltration into the gastric corpus in both sexes. However, leukocyte infiltration was significantly blunted in male mice compared with females (Figure 1*A*–*B*). Immunophenotyping by flow cytometry revealed that macrophage, T cell, and eosinophil infiltration were significantly blunted in *H felis*-infected males compared with females, whereas B cell and neutrophil recruitment were not statistically different between sexes (Figure 1*B*). To further characterize sex differences in the gastric response to *H felis,* we performed bulk RNA sequencing (RNA-seq) on the gastric corpus of infected females and males. Expressed genes from infected females were compared to the expressed genes from infected males. From this comparison, positive differentially expressed genes (DEGs) indicate increased expression in infected females, whereas negative DEGs indicate increased expression in infected males. *H felis* colonization resulted in 2806 differentially activated genes in females compared with 608 activated genes in males. Next, Gene Set Enrichment Analysis (GSEA) was performed using a ranked gene list comparing infected females with infected males to identify pathways differentially enriched between the sexes. Enriched pathways from the Kyoto Encyclopedia of Genes and Genomes (KEGG) and Reactome databases were visualized using ridge plots, where each curve represents the distribution of gene-level ranks contributing to the normalized enrichment score (NES) for a given pathway. In this analysis, positive NES values indicate pathways enriched in infected females relative to infected males. Infected females exhibited broader immune pathway activation and higher enrichment scores, particularly in pathways related to adaptive immunity, antigen presentation, and myeloid cell function (Figure 1*C*). Together, these data demonstrate that females mount a stronger gastric immune response to *Helicobacter* infection compared with males.

Males Are Protected From Helicobacter*-driven Gastric Atrophy and Metaplasia Development*

Chronic inflammation during *Helicobacter* infection drives gastric atrophy and metaplasia development.[29] Given our results demonstrating that males mount blunted immune responses to *H felis* compared with females, we next assessed *Helicobacter*-driven gastric atrophy and metaplasia development. There were no discernible histological differences between mock-infected males and females (Figure 2*A*). *H felis*-infected male mice developed modest chief cell and parietal cell atrophy (Figure 2*A*–*C*). In contrast, female corpus glands exhibited severe remodeling and mucous neck cell hyperplasia, denoted by *Griffonia Simplicifolia II* lectin staining, as well as severe chief and parietal cell atrophy, with near complete loss of both cell types. (Figure 2*A*–*C*). To assess sex differences in PM development, we screened the bulk RNA-seq DEG list described above for a panel of well-described PM-associated transcripts. Among these 14 PM markers, all were significantly expressed at a higher level in infected females compared with infected males (Figure 2*D*). To confirm these results, quantitative reverse transcription polymerase chain reaction (qRT-PCR) was performed for the PM transcripts *Aqp5* and *Gkn3,* both of which were significantly increased in *H felis*-infected females but were not significantly elevated in infected males (Figure 2*E*). Finally, immunostaining for the de novo pyloric metaplasia marker CD44v9 revealed scattered PM-positive gastric units within the male gastric corpus (Figure 2*F*), whereas CD44v9 staining was widespread in *H felis*-infected females. In parallel with increased inflammation, these data demonstrate that *Helicobacter*-infected females develop more severe atrophy and PM compared with infected males.

Sex Differences in Helicobacter *Pathogenesis Are Controlled by Androgens*

Sex hormones play important roles in regulating immune function, and androgens predominately oppose immune activation.[2] We have previously shown that androgen signaling protects the stomach from inflammatory damage.[17] To investigate the physiological mechanisms underlying male protection from *Helicobacter* infection, we castrated adult male mice prior to *H felis* colonization. Two months post-inoculation, immunostaining and flow cytometry revealed that castrated *H felis*-infected mice displayed a significant increase in leukocyte infiltration within the gastric corpus compared with intact infected males (Figure 3*A*–*B*). Moreover, castration significantly increased gastric macrophage and T cell recruitment (Figure 3*B*), which are critical effectors of *Helicobacter*-driven gastric atrophy and PM development.[29,30] We next evaluated how castration impacted *H felis*-driven gastric atrophy and metaplasia development. Hematoxylin and eosin (H&E) micrographs demonstrated that castration dramatically accelerated *H felis* histopathological progression with increased mucous neck cell hyperplasia and gastric atrophy (Figure 3*C*–*D*). Quantification of immunostaining revealed that castration significantly increased chief and parietal atrophy (Figure 3*D*–*E*). Next, qRT-PCR for *Aqp5* and *Gkn3* demonstrated that these PM markers were significantly increased in castrated mice compared with intact infected male controls (Figure 3*F*). Similarly, immunostaining demonstrated a dramatic increase in CD44v9+ gastric units

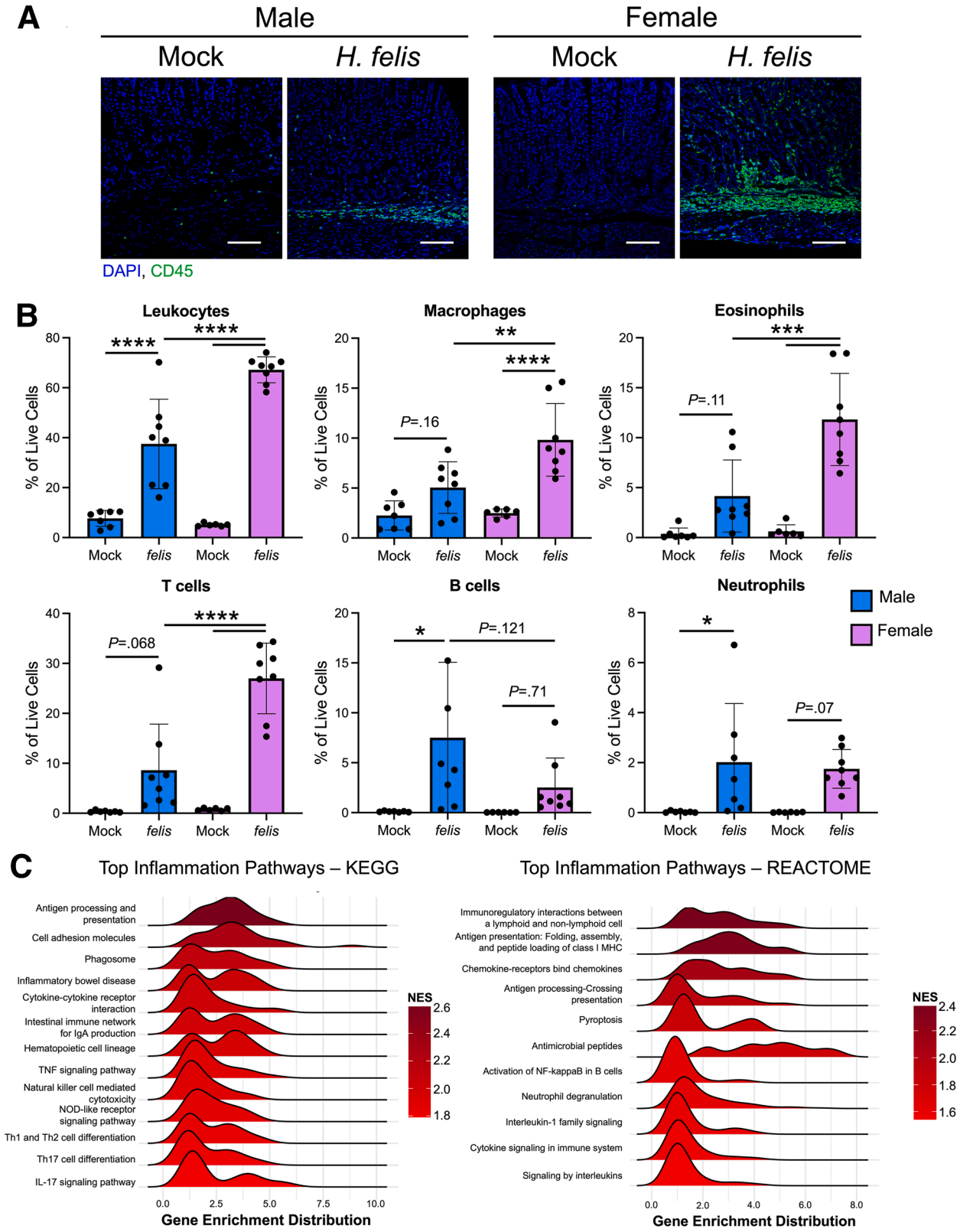

Figure 1. Females mount more intense gastric inflammatory responses to *H felis* infection. (*A*) Representative immunofluorescent staining of CD45+ immune cells (*green*) in the gastric corpus of male and female mice. Nuclei are counterstained with DAPI (*blue*). Scale bars: 100 μm. (*B*) Flow cytometry quantification of the indicated leukocyte populations in the gastric corpus of male and female mice. *$P < .05$; **$P < .01$; ***$P < .001$; ****$P < .0001$. n $\geq$6. (*C*) Ridge plots display of GSEA pathway enrichment. The plots visualize the distribution of ranked gene-level statistics for genes within each enriched pathway, with the density curve representing the relative distribution of genes in the ranked list. n = 3.

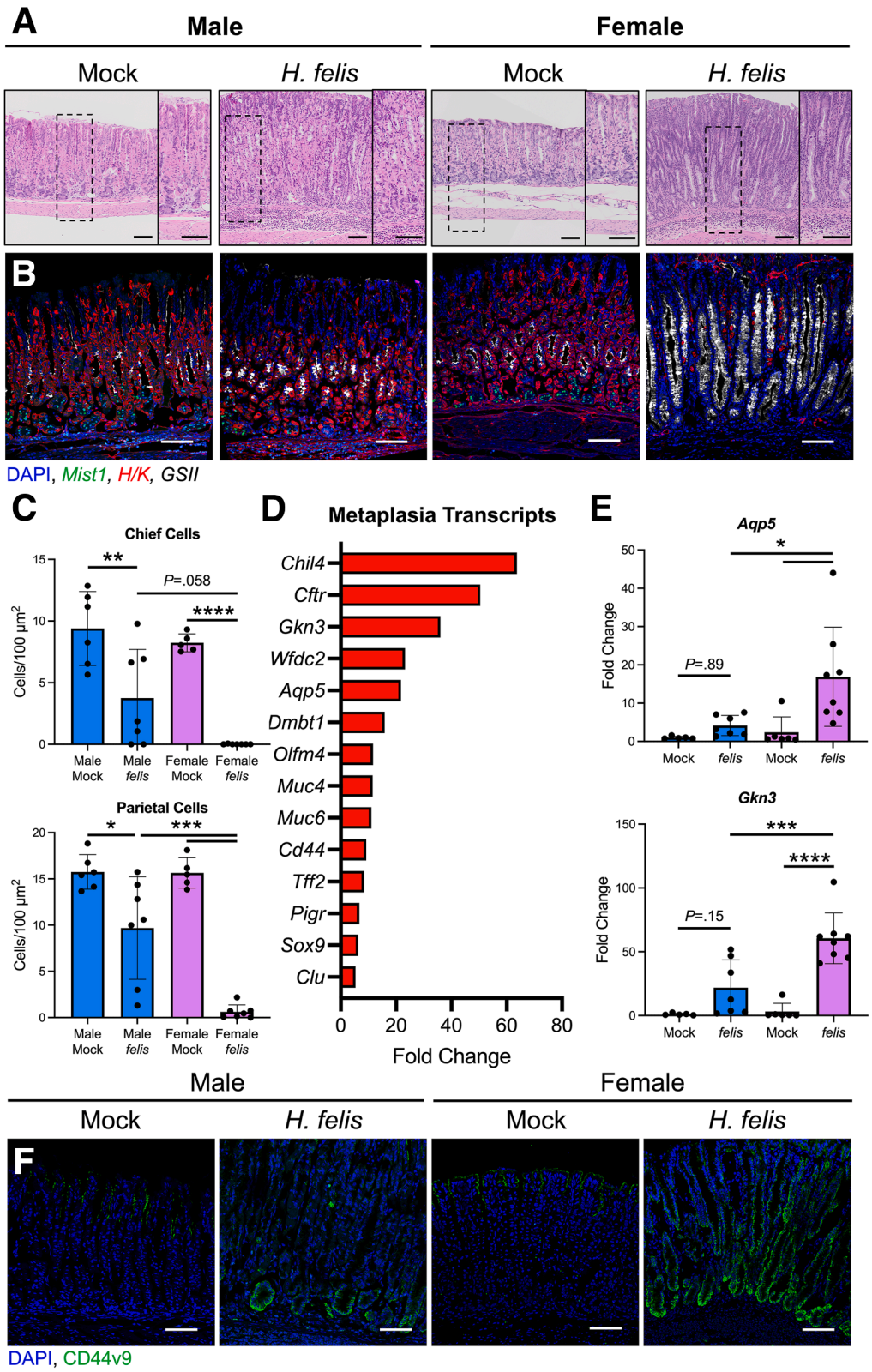

Figure 2. Males are protected from *H felis*-driven gastric atrophy and metaplasia. (*A* and *B*) Representative micrographs of (*A*) H&E-stained sections or (*B*) immunostaining of H+/K+ ATPase (*red*; parietal cells), MIST1 (*green*; chief cells), GSII lectin (*white*; mucous neck cells), and DAPI (*blue*; nuclei) of gastric mucosa from male and female mice 2 months post *H felis* colonization. (*C*) Quantification of chief and parietal cell loss between males and females. (*D*) Fold change of metaplasia-associated genes. The bar plot displays the top-ranked genes associated with metaplasia, ranked by fold change. Gene expression was analyzed and ranked based on differential expression and *P* value. (*E*) qRT-PCR of the metaplasia transcripts *Aqp5* and *Gkn3*. (*F*) Immunofluorescent staining of the metaplastic marker CD44v9 (*green*) in the gastric corpus. All scale bars = 100 μm. *$P < .05$; **$P < .01$; ***$P < .001$; ****$P < .0001$. n $\geq$6, except (*D*) where n = 3.

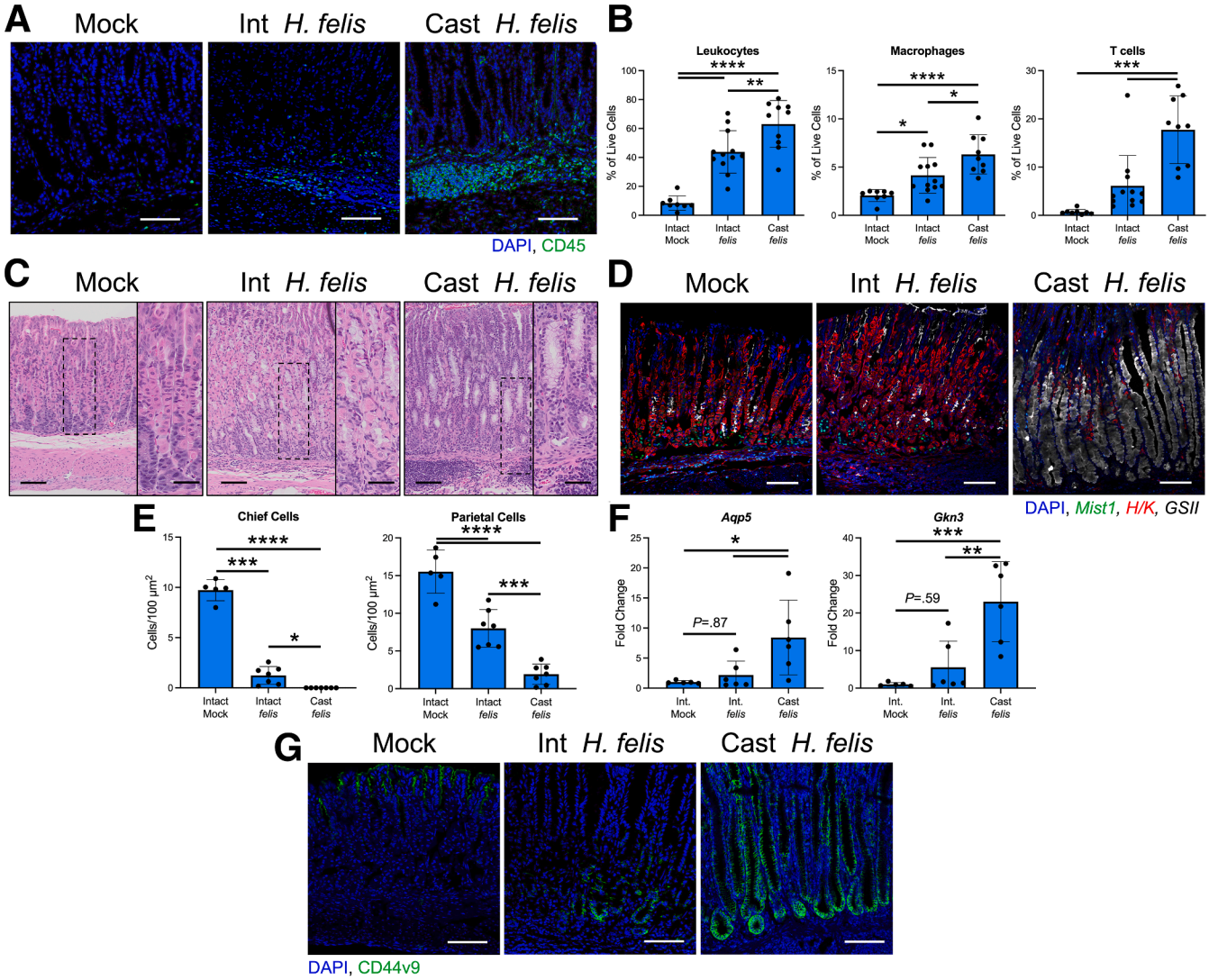

Figure 3. Androgen depletion via castration enhances gastric inflammation and accelerates preneoplastic lesion development. (*A*) Representative immunofluorescent staining of CD45+ immune cells (*green*) in the gastric corpus of male and female mice. Nuclei are counterstained with DAPI (*blue*). (*B*) Flow cytometry quantification of the indicated leukocyte populations in the gastric corpus of intact male and castrated mice 2 months post *H felis* colonization. (*C–D*) Representative micrographs of (*C*) H&E-stained sections or (*D*) immunostaining of H+/K+ ATPase (*red*; parietal cells), MIST1 (*green*; chief cells), GSII lectin (*white*; mucous neck cells), and DAPI (*blue*; nuclei) of gastric mucosa from intact male or castrated male mice. (*E*) Quantification of chief and parietal cell loss. (*F*) qRT-PCR of the metaplasia transcripts *Aqp5* and *Gkn3*. (*G*) Immunofluorescent staining of the metaplastic marker CD44v9 (*green*) in the gastric corpus. Scale bars = 100 μm and 50 μm in the insets (*C*). *$P < .05$; **$P < .01$; ***$P < .001$; ****$P < .0001$. n $\geq$ 5.

(Figure 3*G*). These data demonstrate that castration enhances *H felis*-driven gastric inflammation, atrophy, and metaplasia and suggest that male sex hormones contribute to sex differences in *Helicobacter* pathogenesis.

We next investigated whether androgens protected from *Helicobacter*-induced gastric inflammation, atrophy, and metaplasia by surgically implanting a 5α dihydrotestosterone (DHT) time-release pellet into female mice prior to inoculation with *H felis* (Figure 4*A*). DHT treatment significantly suppressed CD45+ immune cell infiltration compared with placebo-treated *H felis* infected controls (Figure 4*B–C*). Immunophenotyping revealed that DHT treatment significantly suppressed the recruitment of gastric macrophages and T cells (Figure 4*C*). We next evaluated how DHT treatment impacted *H felis*-driven gastric atrophy and metaplasia development. H&E micrographs demonstrated gross remodeling of the gastric mucosa in female *H felis*-infected placebo controls, while remarkably, the stomach of DHT-treated females appeared qualitatively normal (Figure 4*D*). Immunostaining quantification revealed that DHT treatment significantly prevented chief and parietal atrophy compared with placebo-treated controls (Figure 4*D–E*). Next, qRT-PCR for *Aqp5* and *Gkn3* demonstrated that these PM markers were

significantly increased in placebo-treated infected controls, whereas their expression did not significantly increase in infected DHT-treated mice (Figure 4*F*). Similarly, CD44v9 immunostaining was widespread in placebo-treated *H felis*-infected females, whereas staining was undetected in infected females treated with *H felis* (Figure 4*G*). These results demonstrate that androgen suppresses the gastric immune response to *H felis* and protects from subsequent gastric atrophy and PM development.

Androgen-responsive ILC2s Coordinate the Gastric Inflammatory Response to Helicobacter *Infection*

Our results demonstrated that androgens suppress the gastric immune response to *H felis* infection, reducing the recruitment of macrophages and T cells. Androgens primarily signal through the androgen receptor (AR). Therefore, we analyzed our previously described single-cell RNA (scRNA)-seq of gastric leukocytes sorted from the gastric corpus of male, female, and castrated male mice to identify *Ar*+ leukocyte populations.[17] The cells were dimensionally reduced into 9 clusters using the Uniform Manifold Approximation and Projection (UMAP) algorithm (Figure 5*A*). Each cluster was annotated by unique marker signatures, which were depicted in a dot plot (Figure 5*B*). The relative expression of *Ar* transcript density per cell cluster was depicted by violin plot. Three *Ar*+ cell clusters—ILC2s, T cells, and natural killer (NK) cells—were identified, with ILC2s displaying the most ubiquitous expression (Figure 5*C*). Interestingly, the *Ar* was not expressed within the macrophage or dendritic cell clusters, in agreement with our previous findings,[17] despite macrophage recruitment being enhanced following castration and suppressed by DHT treatment (Figures 3*B* and 4*B*, respectively). These results suggest that an androgen-responsive cell type directs macrophage recruitment. Therefore, we mapped communication networks between gastric ILC2s, the APCs macrophages and dendritic cells, and T cells using CellChat. Cell communication scores between ILC2s and APCs were dramatically lower in males compared with females, whereas scores between APCs and T cells were similar between both sexes (Figure 5*D*). Castration dramatically increased the score between ILC2s and APCs, whereas the scores between APCs and T cells remained largely unchanged. These results suggest that ILC2s regulate an APC-T cell axis within the stomach and that androgen signaling suppresses communication between ILC2s and APCs.

ILC2s Initiate an APC-T Cell Axis During Helicobacter *Infection*

Next, we sought to define the leukocyte communication axis that regulates the gastric inflammatory response to *Helicobacter* infection. Based on our scRNA-seq results, we hypothesized that ILC2s regulate the recruitment of macrophages and T cells during *H felis* infection (Figure 6*A*). We employed a genetic approach to deplete either ILC2s or T cells to test this hypothesis. Our scRNA-seq demonstrated that *Il5* is highly restricted to gastric ILC2s (Figure 6*B*). Therefore, we selected the Red5 *Il5* Cre driver to target ILC2s.[31] Although *Helicobacter* infection is predominantly Th1/Th17-polarized, IL5 is also expressed by Th2-polarized T cells.[32–34] Therefore, Red5 Cre mice were colonized with *H felis*, and gastric leukocytes were collected 2 months post-infection. Flow cytometry analysis revealed that tdTomato (IL5) was highly expressed within gastric ILC2s and was not detectable within gastric T cells during infection (Figure 6*C*–*D*). Next, Red5-Cre mice were crossed with a ROSA-DTA Cre-inducible diphtheria toxin to deplete ILC2s (ILC2-DTx). In this mouse model, Cre removes a stop codon, activating diphtheria toxin expression, which induces cell death. Flow cytometry was used to measure gastric ILC2s in ILC2-DTx mice and wild-type (WT) littermate controls, revealing a >4.5-fold reduction in gastric ILC2s (Figure 6*E*).

Next, to define how ILC2 depletion impacted *H felis*-induced gastric inflammation, ILC2-DTx stomachs were assessed by flow cytometry 2 months following *H felis* colonization. Female ILC2-DTx mice exhibited a significant reduction of total gastric leukocyte infiltration compared with female WT littermate controls (Figure 6*F*). Moreover, gastric macrophage and T cell infiltration was significantly reduced, suggesting that ILC2s are required to recruit these cell types following *H felis* colonization. Next, to evaluate the impact of gastric T cell depletion, T cell receptor (TCR) beta/delta double knockout (TCR$\beta\delta$ KO) mice—which lack all mature T cells—were colonized with *H felis* and collected 2 months post-infection. Flow cytometry revealed that total gastric leukocyte infiltration was significantly blunted in female TCR$\beta\delta$ KO mice (Figure 6*G*). However, gastric macrophage infiltration remained significantly elevated. Immunofluorescence imaging indicated that, although macrophages were only a subset of gastric leukocytes in infected female WT controls, nearly all gastric leukocytes were CD68+ macrophages in TCR$\beta\delta$ KO mice (Figure 6*G*–*H*). These results suggest that gastric ILC2s are critical for initiating gastric macrophage and T cell recruitment following *Helicobacter* colonization.

ILC2 Depletion Protects From Helicobacter*-induced Gastric Atrophy and Metaplasia*

ILC2s produce large quantities of Th2-associated cytokines, such as IL13, that are well-known to drive pyloric metaplasia development.[11,12] We have previously reported that androgens suppress cytokine production in ILC2s.[17] Therefore, we next assessed how ILC2 depletion impacted *H felis*-induced gastric atrophy and metaplasia development. Stomachs from ILC2-DTx mice were collected 2 weeks (acute) and 2 months (chronic) post-*H felis* inoculation. Acute *H felis* infection induced significant chief and parietal cell atrophy in WT female mice (Figure 7*A*–*C*). In contrast, *H felis*-infected ILC2-DTx mice were grossly histologically normal and did not exhibit significant changes in the number of chief or parietal cells (Figure 7*A*–*C*). Chronic *H felis* infection induced significant chief and parietal cell atrophy in both female WT and ILC2-DTx mice, but parietal

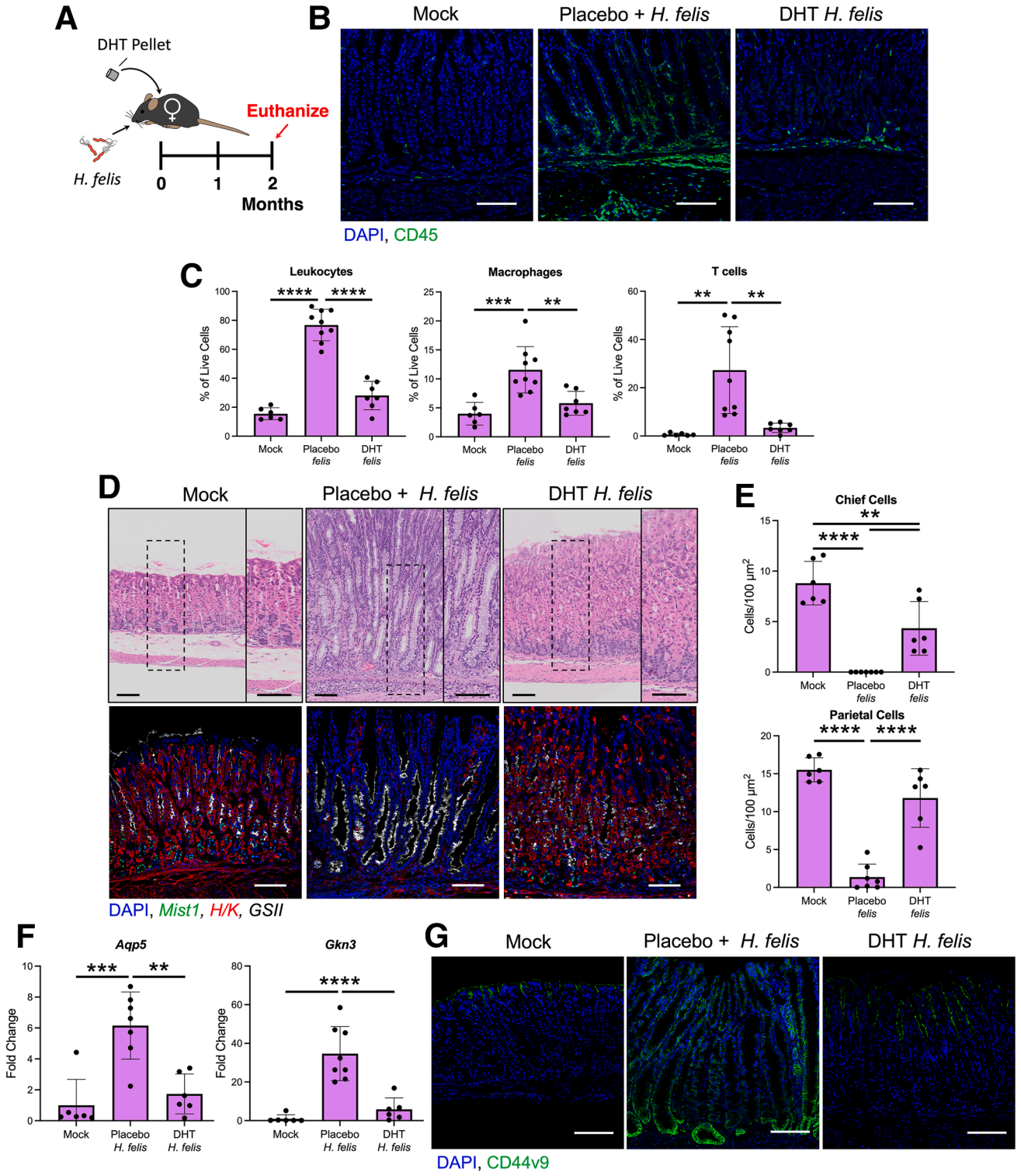

Figure 4. DHT suppresses *H felis* inflammation, atrophy, and metaplasia development. (*A*) Schematic representing experimental design. (*B*) Representative immunofluorescent staining of CD45+ leukocytes (*green*) in the gastric mucosa of mock-inoculated, *H felis*-infected placebo-treated, and DHT-treated female mice. Nuclei are counterstained with DAPI (*blue*). (*C*) Flow cytometry quantification of the indicated leukocyte populations in the gastric corpus. (*D*) Representative micrographs of (*top*) H&E-stained sections or (*bottom*) immunostaining of H+/K+ ATPase (*red*; parietal cells), MIST1 (*green*; chief cells), GSII lectin (*white*; mucous neck cells), and DAPI (*blue*; nuclei) from the gastric corpus. (*E*) Quantification of chief and parietal cell loss. (*F*) qRT-PCR of the metaplasia transcripts *Aqp5* and *Gkn3*. (*G*) Immunofluorescent staining of the metaplastic marker CD44v9 (*green*) in the gastric corpus. All scale bars = 100 μm. $^{**}P < .01$; $^{***}P < .001$; $^{****}P < .0001$. n $\geq$ 6.

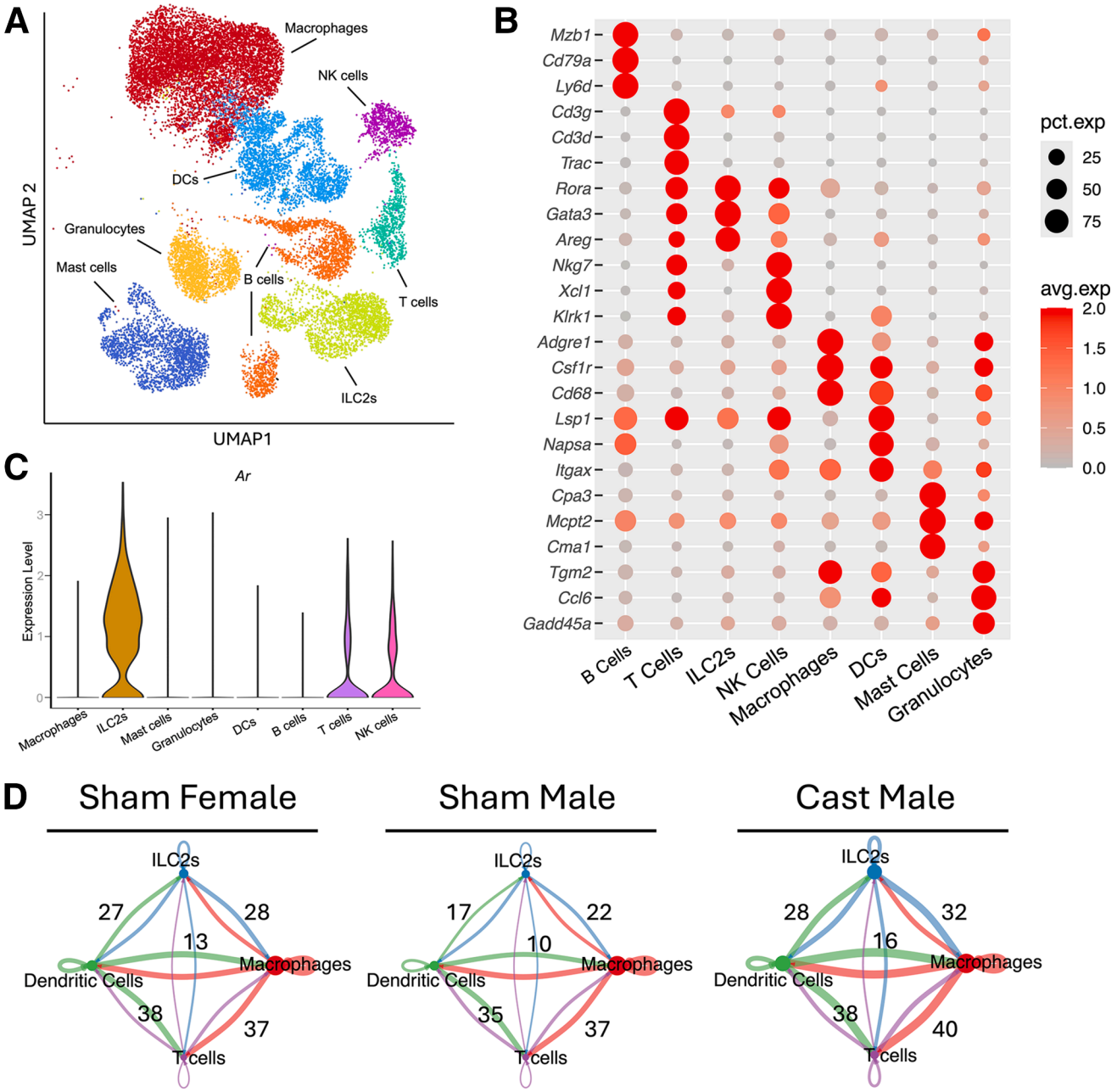

Figure 5. scRNA communication networks predict an androgen responsive ILC2-APC-T cell axis within the gastric immune milieu. (*A*) UMAP plot of immune cell clusters within the gastric corpus of pooled sham female, sham male, and castrated male mice. (*B*) Dot plot showing the expression of key marker genes used to identify immune cell populations. Dot size represents the percentage of cells expressing the gene within each cluster, and dot color indicates the average expression level. (*C*) Violin plot of *Ar* expression across immune cell populations. (*D*) Intercellular communication networks predicted using CellChat. Lines represent ligand-receptor interactions between immune cell populations, with line thickness indicating the strength of interaction. Cells were pooled from 4 individual mice for each group.

cell atrophy was significantly blunted in the ILC2 DTx mice compared with female WT infected controls (Figure 7*A*–*C*). Next, PM development was assessed by qRT-PCR for *Aqp5* and *Gkn3* and by immunostaining for CD44v9. WT infected controls exhibited significant induction of these PM markers at both 2 weeks and 2 months post-infection (Figure 7*D*–*E*). In contrast, increased expression of PM markers was completely ablated in ILC2-DTx mice following acute *H felis* infection and remained significantly reduced following chronic infection (Figure 7*D*–*E*). Finally, immunostaining for CD44v9 demonstrated abundant PM+ gastric units in female WT mice (Figure 7*F*). In contrast, no CD44v9 staining was detected in ILC2-DTx mice 2 weeks post-infection, and scattered PM+ units were present 2

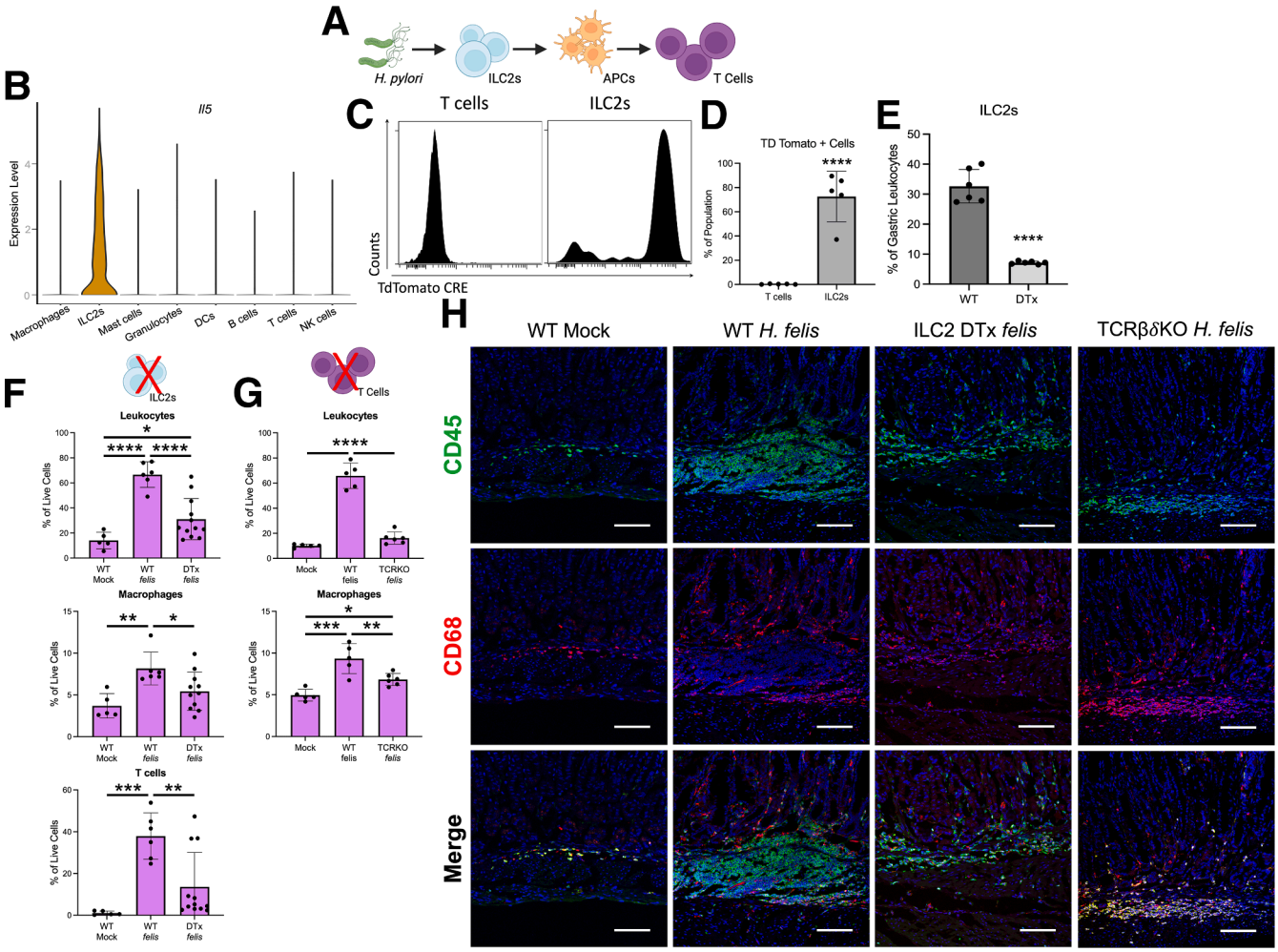

Figure 6. ILC2s control the recruitment of macrophages and T cells during *H felis* infection. (*A*) Schematic depicting putative ILC2-APC-T cell axis. (*B*) Violin plot of *Il5* expression across immune cell populations. (*C–D*) Flow cytometry depicting IL5-tdTomato fluorescence in T cell and ILC2s isolated from Red5-Cre mice 2 months after colonization with *H felis*. (*E*) Flow cytometry quantification of gastric ILC2s in noninfected WT and ILC2 DTx mice. (*F–G*) Flow cytometry quantification of the indicated leukocyte populations in (*F*) TCRBD double KO mice or (*G*) ILC2-DTx mice 2 months after *H felis* colonization. (*H*) Representative immunostaining staining of CD45+ leukocytes (*green*) and the macrophage marker CD68 (*red*) in the gastric mucosa of WT, ILC2-DTx, and TCRB double KO mice. Scale bar: 100 μm. *$P < .05$; **$P < .01$; ***$P < .001$; ****$P < .0001$. n $\geq$ 5.

months post-infection. These data demonstrate that ILC2 depletion protects from *H felis* induced gastric atrophy and metaplasia development.

Discussion

H pylori infection induces chronic gastric inflammation, which damages the mucosa and contributes to several diseases, including gastritis, peptic ulcer disease, and gastric adenocarcinoma. Sex hormones are key regulators of immune responses and contribute to sex disparities in infectious and inflammatory diseases. Sex differences have been reported in several *H pylori*-associated pathologies including gastritis, peptic ulcers, and gastric cancer. However, the direct impact of sex hormones on the gastric inflammatory response to *H pylori* remains poorly understood. In this study, we found that females mounted significantly more robust gastric inflammatory responses than males, primarily due to the immunosuppressive effects of androgen signaling. These findings align with a previous report showing that *H felis*-infected female mice developed more widespread gastritis, epithelial proliferation, and apoptosis compared with males.[35] Although our findings are consistent with broader sex differences in inflammatory responses to infection, clinical studies have reported conflicting associations between sex and *H pylori* pathogenesis. Some studies report a male bias in *H pylori*-associated gastritis and peptic ulcer disease[36,37]; however, these studies do not account for confounding variables such as environmental exposures and lifestyle factors including cigarette smoking and alcohol and red meat consumption—male predominant behaviors that are known to

impact *H pylori* pathogenesis.[38,39] In contrast, a recent study that controlled for smoking and alcohol use found significantly higher monocyte infiltration and a trend toward more severe atrophic gastritis in women.[40] These data suggest that sex differences in *H pylori*-associated gastric disease likely reflect a combination of endogenous factors, such as hormone-mediated immune regulation, and exogenous factors, including sex-linked behavioral patterns. Both should be carefully considered in future studies examining sex-specific outcomes in *H pylori* infection and disease progression.

H pylori is the best-known gastric cancer risk factor. Colonization by *H pylori* elicits a robust but ineffective inflammatory response that fails to eliminate the infection but damages the gastric mucosa and promotes carcinogenesis. The intensity of this immune response directly influences cancer risk, with intense immune responses exacerbating epithelial damage and accelerating dysplastic lesion development.[10] In this study, we found that males mounted weaker inflammatory responses to *H felis* infection compared with females, resulting in less severe gastric atrophy and PM. We further demonstrated that androgens were the primary immune-suppressive hormone driving these sex differences, as castration in males or DHT treatment in females eliminated sex differences in gastric inflammation. These findings align with well-documented sex-based differences in immunity, where males typically mount a weaker immune response to infections than females.

We show here that androgens are anti-inflammatory and protect from sub-chronic gastric atrophy and metaplasia development. Chronic inflammation, atrophy, and metaplasia are pre-dysplastic lesions, but paradoxically, gastric cancer is a male-predominant malignancy, with incidence approximately 2-fold higher in men than in women.[41] Thus, androgen-mediated immune suppression may not be the only factor impacting gastric carcinogenesis. Prior studies have shown that androgens impair wound healing and exacerbate epithelial injury in gastric ulcer models.[42,43] Thus, although androgens may provide short-term protection from inflammation-induced injury, their long-term effects may ultimately favor gastric carcinogenesis. In contrast, estrogens may protect from gastric cancer in females, as previous studies suggest that estrogens confer protection against gastric inflammation and precancerous lesions during *H pylori* infection. Work by Jim Fox's group demonstrated that estrogen depletion in *H pylori*-infected INS-GAS mice increased gastric inflammation and accelerated cancer development, whereas castration had little effect on *H pylori*-induced gastric lesion development.[44–46] Although these findings differ from our current study, such discrepancies may stem from differences in genetic background, as INS-GAS phenotypes are strongly influenced by strain variation as FVB/N INS-GAS mice develop robust gastritis and dysplasia, whereas C57Bl/6 INS-GAS mice develop only mild disease.[47] Thus, future studies should comprehensively define the role of male and female sex hormones in *H pylori*-driven gastric cancer initiation and progression.

ILC2s are tissue-resident leukocytes found in epithelial barrier tissues such as the lungs, skin, and gastrointestinal (GI) tract. In the lungs, androgen signaling in ILC2s contributes to sex differences in asthma and hypersensitivity by suppressing ILC2-mediated inflammation and type 2 cytokine production.[22,48] We previously reported that androgen treatment suppresses cytokine transcription in ILC2s, and that ILC2 depletion protects the stomach from adrenalectomy-induced spontaneous gastric inflammation, atrophy, and PM.[17] In this study, we identified that ILC2s are critical regulators of sex differences in the gastric inflammatory response to *Helicobacter* infection. Similar findings have recently been reported in the skin, where androgen signaling regulates an ILC2-dendritic cell-T cell axis to suppress inflammatory responses in males following bacterial infection.[24] That study identified granulocyte-macrophage colony-stimulating factor (GM-CSF) as the key effector molecule by which ILC2s directed dendritic cell activation. Similar mechanisms likely operate in the stomach, as we previously showed that androgens regulate *Csf2* (which encodes GM-CSF) transcription in ILC2s, and that gastric macrophages and dendritic cells express the GM-CSF co-receptors *Csf2ra* and *Csf2rb*.[17] Collectively, these results indicate that gastric ILC2s are critical regulators of gastric inflammation, controlling APC recruitment and activation following gastric injury or *Helicobacter* colonization.

PM is a reactive lesion that develops in the gastric corpus in response to glandular injury. PM initially develops as part of a wound healing response, during which post-mitotic chief cells transdifferentiate into proliferative, mucous-producing cells.[49] Under conditions of transient injury, these metaplastic cells are replaced as normal glandular architecture is restored. However, with chronic insult, PM develops an intestinal phenotype and may eventually transition to intestinal metaplasia or directly to dysplasia.[50–52] Cytokines produced by immune cells play a critical role in directing epithelial cell fate and regeneration, highlighting the role of immune-epithelial crosstalk in shaping disease outcomes. IL13, produced in the stomach by mast cells and ILC2s, drives PM maturation, both directly through activation of STAT6 signaling in chief cells, and indirectly by signaling in tuft cells.[11,12,53] Several studies have reported that ILC2 depletion suppresses PM development.[17,18,53] Consistent with these findings, we demonstrated here that ILC2 depletion protected from *H felis*-induced PM. This reduction likely stems from both decreased inflammatory intensity and diminished IL13 levels required to drive PM maturation. Our results show that androgens are upstream of the ILC2-IL13-PM cascade, regulating sex differences in PM development following gastric injury.

In summary, this study highlights the importance of investigating sex differences in *H pylori* pathogenesis. Our findings reveal a novel role for androgens in regulating gastric inflammation through an ILC2-macrophage-T cell axis. We demonstrate that androgen depletion enhances the gastric inflammatory response to *Helicobacter* infection and accelerates pre-dysplastic lesion development.

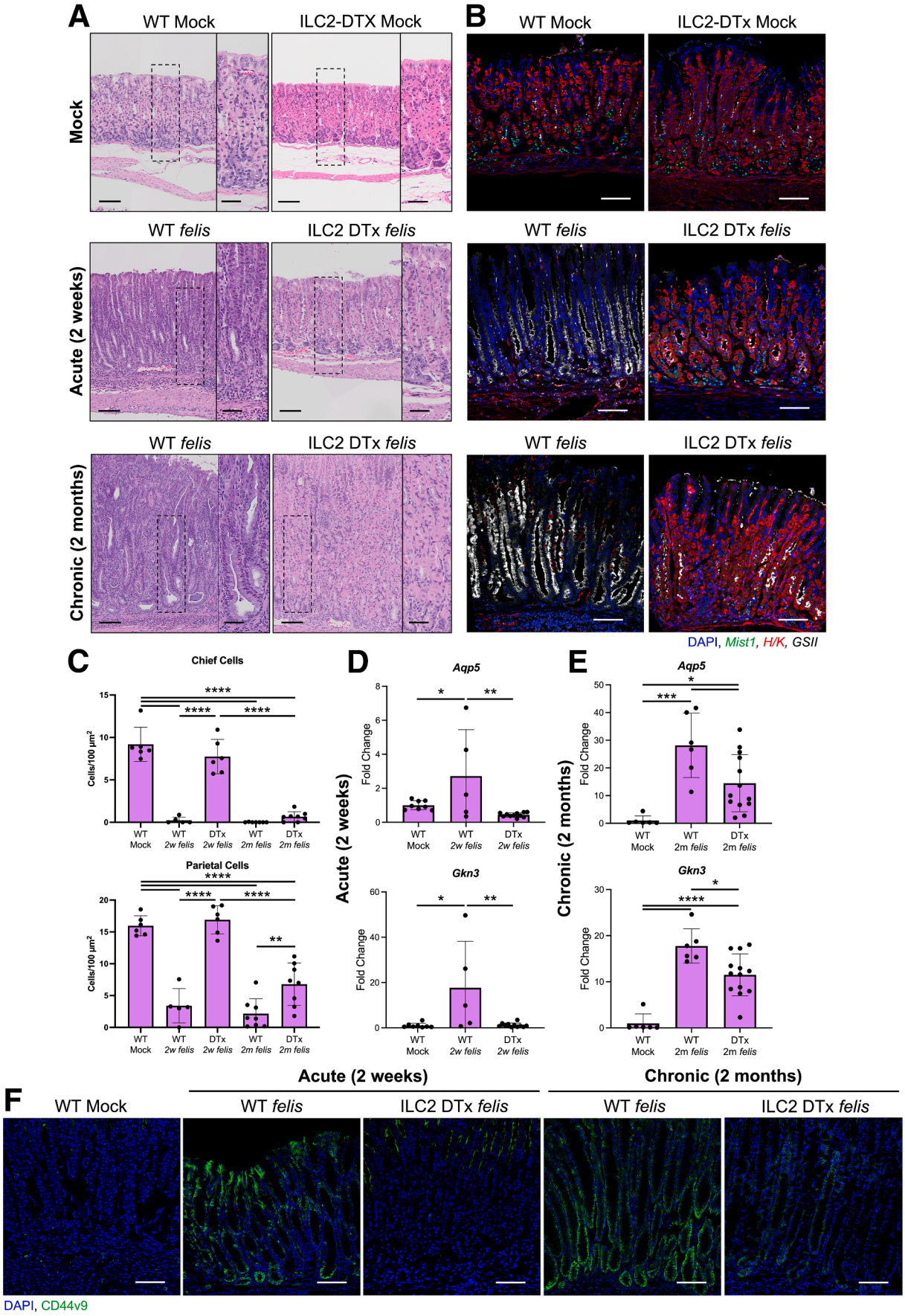
A
WT Mock
ILC2-DTX Mock
Mock
WT felis
ILC2 DTx felis
Acute (2 weeks)
Chronic (2 months)
B
WT Mock
ILC2-DTx Mock
DAPI, Mist1, H/K, GSII
C
Chief Cells
Parietal Cells
Cells/100 µm²
WT Mock
WT 2w felis
DTx 2w felis
WT 2m felis
DTx 2m felis
D
Aqp5
Gkn3
Fold Change
Acute (2 weeks)
E
Chronic (2 months)
F
Acute (2 weeks)
Chronic (2 months)
DAPI, CD44v9

Although cancer development was not directly assessed in this study, our results have important implications for cancer risk, suggesting that androgen regulation of gastric immune responses may have long-term consequences for disease progression and contribute to sex disparities in gastric cancer.

Material and Methods

Animal Care and Treatment

C57BL/6J, TCR$\beta\delta$KO (strain number 002122), ROSA-DTA (strain number 009669), and Red5 (strain number 030926) mice were purchased from the Jackson Laboratory. Mice were administered standard chow and water ad libitum and maintained in a temperature- and humidity-controlled room with standard 12-hour light/dark cycles. The TCR$\beta\delta$KO strain was maintained in sterile housing for immunocompromised mice. The ROSA-DTA and Red5-Cre were crossed to constitutively deplete IL5-expressing cells. Mice with the genotype ROSA-DTA; *Il5* Cre+/− were considered ILC2 deficient (called ILC2 DTx hereafter), whereas mice with the genotype ROSA-DTA; *Il5* Cre −/− were used as WT littermate controls. Eight-week-old mice were used for all experiments. Mock mice received 500 μL sterile brucella broth, and infected mice were inoculated with 500 μL of brucella broth containing 10^9 colony-forming units (CFU) of the bacteria 2 times 24 hours apart as previously described.[26] Castration and drug pellet implantation were performed as previously described.[17]

Study Approvals

All mouse studies were performed with approval by the West Virginia University Animal Care and Use Committee.

Bacteria Preparation

H felis (ATCC 49179) was grown on tryptic soy agar plates (BD Biosciences) with 5% defibrinated sheep blood (Hemostat Labs) and 10 μg/mL vancomycin (Alfa Aesar) under microaerophilic conditions (5% O_2 and 10% CO_2) at 37°C for 2 days. *H felis* was then harvested and transferred to Brucella broth (Research Products International) containing 5% fetal bovine serum (FBS; R&D Systems) and 10 μg/mL vancomycin and grown overnight at 37°C under microaerophilic conditions with agitation. Bacteria were centrifuged and resuspended in fresh Brucella broth without antibiotics before spectrophotometry and mouse infection.

Tissue Preparation

Stomachs were opened along the greater curvature and washed in phosphate buffered saline (PBS) to remove the gastric contents. Stomachs used for histology were pinned to cork boards and fixed overnight in 4% paraformaldehyde at 4°C. For histology, strips were taken from the greater curvature of the gastric corpus. Stomach strips were then transferred into 70% ethanol and submitted to the West Virginia University histology core for routine processing, embedding, sectioning, and H&E staining. Images were obtained using an Olympus VS-120 brightfield slide scanning microscope. Stomachs used for immunostaining were obtained from the lessor curvature and cryopreserved in 30% sucrose and then embedded in optimal cutting temperature media.

Immunohistochemistry

Immunostaining was performed using standard methods. Briefly, 5-μm stomach cryosections were incubated with anti H+/K+ ATPase antibodies (clone 1H9, MBL Life Science), MIST1 (clone D7N4B; Cell Signaling Technologies), CD45 (clone 104; Biolegend), CD68 (clone FA-11; Biolegend), or CD44v9 (Cosmo Bio) for 1 hour at room temperature or overnight at 4°C. Sections were incubated in secondary antibodies for 1 hour at room temperature. Fluorescence-conjugated *Griffonia simplicifolia* lectin (GSII; ThermoFisher) was added with secondary antibodies where indicated. Sections were mounted with Vectastain mounting media containing 4′,6-diamidino-2-phenylindole (Vector Laboratories). Images were obtained using a Zeiss 710 confocal laser-scanning microscope (Carl-Zeiss) and running Zen Black (Carl-Zeiss) imaging software. Parietal cells and chief cells were quantitated as previously described[30] using confocal micrographs captured with a ×20 microscope objective. Cells were counted using the ImageJ count tool (National Institutes of Health). Cells that stained positive with anti-H^+-K^+ antibodies were identified as parietal cells, and cells that stained positive with anti-MIST1 antibodies and were GSII-negative were identified as mature chief cells. Cell counts were normalized to image area to determine the cell number per 100 μm^2. Images that contained gastric glands cut longitudinally were selected for counting. For each mouse, 2 nonoverlapping fields were analyzed to establish cell counts, and the average from these 2 fields was used to represent a single biological replicate. Each data point reflects the mean quantification from 2 fields per individual mouse.

Figure 7. (***See previous page***). **ILC2 depletion protects against *H felis*-induced gastric atrophy and metaplasia.** (*A*) Representative micrographs of H&E staining of the gastric corpus of acute (2 week) and chronic (2 month) infected WT and ILC2-deficient (DTx) mice. (*B*) Representative immunofluorescent staining of corpus tissue probed with H+/K+ ATPase (*red*; parietal cells), MIST1 (*green*; chief cells), and GSII lectin (*white*; mucous neck cells) in the gastric mucosa. Nuclei are counterstained with DAPI (*blue*). Scale bar: 100 μm. (*C*) Quantitation of chief and parietal cell loss between WT and ILC-DTx females at 2 weeks and 2 months per 20× field. (*D–E*) qRT-PCR analysis of the metaplastic markers *Aqp5* and *Gkn3* in ILC2-DTx mice (*D*) 2 weeks and (*E*) 2 months post *H felis*-colonization. (*F*) Immunofluorescent staining of the metaplastic marker CD44v9 (*green*). All scale bars = 100 μm. *$P < .05$; **$P < .01$; ***$P < .001$; ****$P < .0001$. n $\geq$ 5.

RNA Isolation and qRT-PCR

Gastric tissue RNA biopsies were collected from the greater curvature using a 2-mm biopsy punch. RNA was extracted in TRIzol (Thermo Fisher Scientific) and precipitated from the aqueous phase using 1 volume of 100% ethanol. The mixture was transferred to an RNA isolation column (Omega Bio-Tek), and the remaining steps were followed according to the manufacturer's recommendations. RNA was treated with RNase-free DNase I (Omega Bio-Tek) as part of the isolation procedure. Reverse transcription followed by qPCR was performed in the same reaction using the Universal Probes One-Step PCR kit (Bio-Rad Laboratories) and the TaqMan primers/probe mixtures (all from Thermo Fisher Scientific): *Ppib* (Mm00478295_m1), *Aqp5* (Mm00437578_m1), *Gkn3* (Mm01183934_m1).

Flow Cytometry

Corpus tissue from euthanized mice was washed in Hanks' Balanced Salt Solution (HBSS) without Ca^{2+} or Mg^{2+} containing 5 mM HEPES, 5 mM EDTA, and 5% FBS at 37°C plus 1 μL/mL dithiothreitol. Tissue was then washed in HBSS with Ca^{2+} or Mg^{2+} and then digested in 1 mg/mL collagenase (Worthington Biochemical). After digestion, the tissue fragments were pushed through a 100-μM strainer and centrifuged. Pelleted cells were resuspended and rinsed through a 40-μM strainer. Intact cells were enriched using an Optiprep (Serumwerk) density gradient. Fc receptors were blocked with TruStain (Biolegend) and then stained with antibodies. The following antibodies were used: CD45.2 (clone 104), CD3e (clone 145-2C11), B220 (clone RA3-6B2), CD4 (clone GK1.5), CD8a (clone 53-6.7), CD11b (clone M1/70), MHCII (clone M5/114.15.2), Ly6g (clone 1A8), F4/80 (clone BM8), SiglecF (clone E50-2440), Lineage cocktail (Biolegend), CD127 (clone A7R34), Ly-6A/E Sca-1 (clone D7), ICOS (clone 15F9). Actinomycin D (clone A1310, Invitrogen) was used to label dead cells. Super Bright Complete staining buffer (Invitrogen) was used in antibody cocktails containing multiple brilliant violet fluorophores. Cells were analyzed on a Cytek Aurora spectral flow cytometer (Cytek Biosciences). Flow cytometry analysis was performed using Cytobank analysis software (Beckman Coulter).

RNA-seq

Helicobacter felis-infected female and male mice were euthanized 2 months post-inoculation. The gastric corpus was harvested, and RNA was isolated as previously described. RNA libraries were prepared using a NEB Ultra II Directional RNA Library Prep Kit with poly-A selection (Admera Health). Sequencing was performed on a paired-end platform, generating 150-bp reads with a depth of 40 million reads per sample. Following sequencing, the West Virginia University Bioinformatics Core processed the raw data to generate a list of DEGs and a reads per kilobase per million (RPKM) file. The DEG list included log2 fold change (logFC), adjusted P values, and other statistical metrics. Transcript data was deposited at the Gene Expression Omnibus; accession number: GSE293519.

GSEA

GSEA was performed using the clusterProfiler and REACTOMEPA packages in R to identify significantly enriched pathways associated with immune-related processes. All truly DEGs were ranked by logFC derived from differential gene expression analysis. Both mouse-specific KEGG and REACTOME gene sets were utilized for the analysis. For KEGG pathway analysis, the gseKEGG function was applied with the following parameters: a minimum gene set size of 10, a maximum size of 500, and a significance threshold of adjusted $P < .05$. REACTOME pathway analysis was conducted using the gsePathway function in the REACTOMEPA package. Parameters included a minimum gene set size of 10, a maximum size of 500, and a significance threshold of adjusted $P < .05$. The KEGG database and REACTOME database-specific annotations were mapped to mouse-specific Entrez IDs. GSEA data was visualized using Ridgeline plots. The plots indicate the GSEA pathway normalized enrichment score and the distribution of ranked genes that contribute to pathway activation.

scRNA-seq

Previously published scRNA-seq datasets were used for this study.[17] H5 files were downloaded from the National Center for Biotechnology Informatio Gene Expression Omnibus, GSE147177 and imported into R (version 4.3.3). The files contain scRNA-seq data from pooled (n = 4) CD45+ leukocytes isolated from the gastric corpus of normal males, normal females, and adrenalectomized + castrated males. Gene expression matrices were converted into a Seurat object using the Seurat R package (version 5.0.3). Gene expression measurements were normalized using the Seurat NormalizeData function and standardized using ScaleData. Next, genes that expressed high variability across cells were identified using Seurat's FindVariableFeatures function. The Seurat RunPCA function and visualization of the components via elbow plot were performed, and the first 20 components were selected for further analyses. The RunUMAP, dimensions = 20, min.distance = .5 and n.neighbors= 20, function was then applied and the FindNeighbors function was used using the first 20 dimensions to construct a Shared Nearest Neighbor Graph. FindClusters with "resolution = .5" was performed to cluster cells into respective clusters. All marker genes with a minimum .4 pct expression value were identified using Seurat's FindAllMarkers function and exported to an excel table. Additionally, UMAP plots were converted to a loupe file using 10XGenomics Loupe Browser using the create_loupe_fromSeurat function. Annotation and color visualization was performed in Loupe Browser (version 8.0.0). Marker genes were identified by the average expression value in the cluster of interest and had a minimum pct value of .8 or higher while the minimum pct was below .4. This insured high expression of the gene profile

within the cluster while limiting the expression in the other clusters. Once clusters were identified, gene matrices were subsetted using the subset.data function to include only the clusters of interest for further analysis.

Communication Networks

Subsetted Seurat objects containing the gene expression matrices were converted into a cell chat object using CellChat's (version 2.1.2) createCellChatobject function. CellChat's identifyOverExpressedGenes function was used to find overexpressed genes in clusters of interest using CellChat's mouse data bank. Ligand-receptor pairs were identified using CellChat's identifyOverExpressedInteractions to further analyze cell communication. A communication probability matrix was generated using the computeCommunProb function using the TriMean to calculate probability scores. Once calculated, communication networks were visualized using CellChat's netVisual_circle function.

Statistical Analysis

All error bars are ± standard deviation (SD) of the mean. The sample size for each experiment is indicated in the figure legends. Experiments were repeated a minimum of 2 times. Statistical analyses were performed using 1-way analysis of variance (ANOVA) with the post hoc Tukey t-test when comparing 3 or more groups or by an unpaired *t*-test when comparing 2 groups. Statistical analysis was performed by GraphPad Prism 10 software. Statistical significance was set at $P \leq .05$. Specific P values are listed in the figure legends.

References

1. Klein SL, Flanagan KL. Sex differences in immune responses. Nat Rev Immunol 2016;16:626–638.
2. Trigunaite A, Dimo J, Jørgensen TN. Suppressive effects of androgens on the immune system. Cell Immunol 2015;294:87–94.
3. Wilkinson NM, Chen HC, Lechner MG, Su MA. Sex differences in immunity. Annu Rev Immunol 2022;40:75–94.
4. Bray F, Laversanne M, Sung H, et al. Global cancer statistics 2022: GLOBOCAN estimates of incidence and mortality worldwide for 36 cancers in 185 countries. CA Cancer J Clin 2024;74:229–263.
5. Thrift AP, Wenker TN, El-Serag HB. Global burden of gastric cancer: epidemiological trends, risk factors, screening and prevention. Nat Rev Clin Oncol 2023;20:338–349.
6. Hitzler I, Kohler E, Engler DB, et al. The role of Th cell subsets in the control of Helicobacter infections and in T cell-driven gastric immunopathology. Front Immunol 2012;3:142.
7. Serrano C, Wright SW, Bimczok D, et al. Downregulated Th17 responses are associated with reduced gastritis in Helicobacter pylori-infected children. Mucosal Immunol 2013;6:950–959.
8. Osaki LH, Bockerstett KA, Wong CF, et al. Interferon-γ directly induces gastric epithelial cell death and is required for progression to metaplasia. J Pathol 2019;247:513–523.
9. Fukui T, Nishio A, Okazaki K, et al. Cross-primed CD8+ cytotoxic T cells induce severe Helicobacter-associated gastritis in the absence of CD4+ T cells. Helicobacter 2007;12:486–497.
10. Arnold IC, Lee JY, Amieva MR, et al. Tolerance rather than immunity protects from Helicobacter pylori-induced gastric preneoplasia. Gastroenterology 2011;140:199–209.
11. Noto CN, Hoft SG, Bockerstett KA, et al. IL13 acts directly on gastric epithelial cells to promote metaplasia development during chronic gastritis. Cell Mol Gastroenterol Hepatol 2022;13:623–642.
12. Contreras-Panta EW, Lee SH, Won Y, et al. Interleukin 13 promotes maturation and proliferation in metaplastic gastroids. Cell Mol Gastroenterol Hepatol 2024;18:101366.
13. O'Reilly LA, Putoczki TL, Mielke LA, et al. Loss of NF-κB1 causes gastric cancer with aberrant inflammation and expression of immune checkpoint regulators in a STAT-1-dependent manner. Immunity 2018;48:570–583.e8.
14. Tu S, Bhagat G, Cui G, et al. Overexpression of interleukin-1beta induces gastric inflammation and cancer and mobilizes myeloid-derived suppressor cells in mice. Cancer Cell 2008;14:408–419.
15. Lindblad M, Rodríguez LA, Lagergren J. Body mass, tobacco and alcohol and risk of esophageal, gastric cardia, and gastric non-cardia adenocarcinoma among men and women in a nested case-control study. Cancer Causes Control 2005;16:285–294.
16. Freedman ND, Derakhshan MH, Abnet CC, et al. Male predominance of upper gastrointestinal adenocarcinoma cannot be explained by differences in tobacco smoking in men versus women. Eur J Cancer 2010;46:2473–2478.
17. Busada JT, Peterson KN, Khadka S, et al. Glucocorticoids and androgens protect from gastric metaplasia by suppressing group 2 innate lymphoid cell activation. Gastroenterology 2021;161:637–652.e4.
18. Meyer AR, Engevik AC, Madorsky T, et al. Group 2 innate lymphoid cells coordinate damage response in the stomach. Gastroenterology 2020;159:2077–2091.e8.
19. Petersen CP, Meyer AR, De Salvo C, et al. A signalling cascade of IL-33 to IL-13 regulates metaplasia in the mouse stomach. Gut 2018;67:805–817.
20. Klein Wolterink RG, Kleinjan A, van Nimwegen M, et al. Pulmonary innate lymphoid cells are major producers of IL-5 and IL-13 in murine models of allergic asthma. Eur J Immunol 2012;42:1106–1116.
21. de Lucía Finkel P, Xia W, Jefferies WA. Beyond unconventional: what do we really know about group 2 innate lymphoid cells? J Immunol 2021;206:1409–1417.
22. Cephus JY, Stier MT, Fuseini H, et al. Testosterone attenuates group 2 innate lymphoid cell-mediated airway inflammation. Cell Rep 2017;21:2487–2499.

23. Blanquart E, Mandonnet A, Mars M, et al. Targeting androgen signaling in ILC2s protects from IL-33-driven lung inflammation, independently of KLRG1. J Allergy Clin Immunol 2022;149:237–251.e12.
24. Chi L, Liu C, Gribonika I, et al. Sexual dimorphism in skin immunity is mediated by an androgen-ILC2-dendritic cell axis. Science 2024;384:eadk6200.
25. Satoh-Takayama N, Kato T, Motomura Y, et al. Bacteria-induced group 2 innate lymphoid cells in the stomach provide immune protection through induction of IgA. Immunity 2020;52:635–649.e4.
26. Druffner SR, Venkateshwaraprabu S, Khadka S, et al. Comparison of gastric inflammation and metaplasia induced by Helicobacter pylori or Helicobacter felis colonization in mice. Microbiol Spectr 2024;12:e0001524.
27. Zhang S, Moss SF. Rodent models of Helicobacter infection, inflammation, and disease. Methods Mol Biol 2012;921:89–98.
28. Hoft SG, Noto CN, DiPaolo RJ. Two distinct etiologies of gastric cancer: infection and autoimmunity. Front Cell Dev Biol 2021;9:752346.
29. Roth KA, Kapadia SB, Martin SM, Lorenz RG. Cellular immune responses are essential for the development of Helicobacter felis-associated gastric pathology. J Immunol 1999;163:1490–1497.
30. Busada JT, Ramamoorthy S, Cain DW, et al. Endogenous glucocorticoids prevent gastric metaplasia by suppressing spontaneous inflammation. J Clin Invest 2019;129:1345–1358.
31. Nussbaum JC, Van Dyken SJ, von Moltke J, et al. Type 2 innate lymphoid cells control eosinophil homeostasis. Nature 2013;502:245–248.
32. Upadhyaya B, Yin Y, Hill BJ, et al. Hierarchical IL-5 expression defines a subpopulation of highly differentiated human Th2 cells. J Immunol 2011; 187:3111–3120.
33. Eaton KA, Benson LH, Haeger J, Gray BM. Role of transcription factor T-bet expression by CD4+ cells in gastritis due to Helicobacter pylori in mice. Infect Immun 2006;74:4673–4684.
34. Freire de Melo F, Rocha GA, Rocha AM, et al. Th1 immune response to H. pylori infection varies according to the age of the patients and influences the gastric inflammatory patterns. Int J Med Microbiol 2014; 304:300–306.
35. Court M, Robinson PA, Dixon MF, et al. The effect of gender on Helicobacter felis-mediated gastritis, epithelial cell proliferation, and apoptosis in the mouse model. J Pathol 2003;201:303–311.
36. Kato S, Matsukura N, Togashi A, et al. Sex differences in mucosal response to Helicobacter pylori infection in the stomach and variations in interleukin-8, COX-2 and trefoil factor family 1 gene expression. Aliment Pharmacol Ther 2004;20(Suppl 1):17–24.
37. Kodama M, Okimoto T, Mizukami K, et al. Gastric mucosal changes, and sex differences therein, after Helicobacter pylori eradication: a long-term prospective follow-up study. J Gastroenterol Hepatol 2021; 36:2210–2216.
38. Morris MT, Duncan BC, Piazuelo MB, et al. Chronic cigarette smoke exposure masks pathological features of Helicobacter pylori infection while promoting tumor initiation. Cancer Prev Res (Phila) 2025;18:271–281.
39. Tan MC, Mallepally N, Nguyen TH, et al. Missed opportunities for screening or surveillance among patients with newly diagnosed non-cardia gastric adenocarcinoma. Dig Dis Sci 2023;68:761–769.
40. Kim HJ, Kim N, Jang JY, et al. Influence of cytokine genetic polymorphisms in helicobacter pylori-associated gastric inflammation according to sex in South Korea. Gut Liver 2024;18:1002–1013.
41. Jackson SS, Marks MA, Katki HA, et al. Sex disparities in the incidence of 21 cancer types: quantification of the contribution of risk factors. Cancer 2022; 128:3531–3540.
42. Machowska A, Brzozowski T, Sliwowski Z, et al. Gastric secretion, proinflammatory cytokines and epidermal growth factor (EGF) in the delayed healing of lingual and gastric ulcerations by testosterone. Inflammopharmacology 2008;16:40–47.
43. Machowska A, Szlachcic A, Pawlik M, et al. The role of female and male sex hormones in the healing process of preexisting lingual and gastric ulcerations. J Physiol Pharmacol 2004;55(Suppl 2):91–104.
44. Ohtani M, Ge Z, García A, et al. 17 β-estradiol suppresses Helicobacter pylori-induced gastric pathology in male hypergastrinemic INS-GAS mice. Carcinogenesis 2011;32:1244–1250.
45. Sheh A, Ge Z, Parry NM, et al. 17β-estradiol and tamoxifen prevent gastric cancer by modulating leukocyte recruitment and oncogenic pathways in Helicobacter pylori-infected INS-GAS male mice. Cancer Prev Res (Phila) 2011;4:1426–1435.
46. Ohtani M, García A, Rogers AB, et al. Protective role of 17 beta -estradiol against the development of Helicobacter pylori-induced gastric cancer in INS-GAS mice. Carcinogenesis 2007;28:2597–2604.
47. Takaishi S, Tu S, Dubeykovskaya ZA, et al. Gastrin is an essential cofactor for helicobacter-associated gastric corpus carcinogenesis in C57BL/6 mice. Am J Pathol 2009;175:365–375.
48. Laffont S, Blanquart E, Savignac M, et al. Androgen signaling negatively controls group 2 innate lymphoid cells. J Exp Med 2017;214:1581–1592.
49. Goldenring JR, Mills JC. Cellular plasticity, reprogramming, and regeneration: metaplasia in the stomach and beyond. Gastroenterology 2022;162:415–430.
50. Hoft SG, Brennan M, Carrero JA, et al. Unveiling cancer-related metaplastic cells in both helicobacter pylori infection and autoimmune gastritis. Gastroenterology 2025;168:53–67.
51. Lee SH, Jang B, Min J, et al. Up-regulation of aquaporin 5 defines spasmolytic polypeptide-expressing metaplasia and progression to incomplete intestinal metaplasia. Cell Mol Gastroenterol Hepatol 2022;13:199–217.
52. Cho CJ, Brown JW, Mills JC. Origins of cancer: ain't it just mature cells misbehaving? EMBO J 2024; 43:2530–2551.

53. O'Keefe RN, Carli ALE, Baloyan D, et al. A tuft cell - ILC2 signaling circuit provides therapeutic targets to inhibit gastric metaplasia and tumor development. Nat Commun 2023;14:6872.

Received August 18, 2025. Accepted November 20, 2025.

Correspondence
Address correspondence to: Jonathan T. Busada, PhD, WVU School of Medicine, Microbiology, Immunology and Cell Biology, 64 Medical Center Drive, P.O. Box 9177, Morgantown, West Virginia 26506. e-mail: jonathan.busada@hsc.wvu.edu.

Acknowledgments
The authors thank Dr Richard DiPaolo for critical reading of the manuscript.

CRediT Authorship Contributions

Benjamin C. Duncan (Conceptualization: Equal; Data curation: Lead; Formal analysis: Equal; Investigation: Lead; Visualization: Equal; Writing – original draft: Equal; Writing – review & editing: Equal)

Maeve T. Morris (Data curation: Supporting; Formal analysis: Supporting; Investigation: Supporting; Writing – review & editing: Supporting)

Jordan L. Pascoe (Data curation: Supporting; Investigation: Supporting)

Stuti Khadka (Data curation: Supporting; Investigation: Supporting)

Lei Wang (Data curation: Supporting; Investigation: Supporting)

Gangqing Hu (Data curation: Supporting; Investigation: Supporting)

Jonathan T. Busada, PhD (Conceptualization: Lead; Data curation: Supporting; Formal analysis: Equal; Funding acquisition: Lead; Supervision: Lead; Writing – original draft: Lead; Writing – review & editing: Lead)

Conflicts of interest
The authors disclose no conflicts.

Funding
This work was supported by West Virginia University start-up funds and from the West Virginia University Cancer Institute (Jonathan T. Busada).

The West Virginia University Microscope Imaging Facility, Flow Cytometry & Single Cell Core, and Genomics Core Facility receive support from the National Institutes of Health grants P30GM103503 and S10 grant OD028605, and U54 GM104942 respectively. The West Virginia University Bioinformatics Core Facility is supported by National Institutes of Health grants U54GM104942 and P20GM103434.

Data Availability
Sequencing data can be accessed at the NCBI GEO repository. The accession number for the bulk RNA sequencing is GSE29351. The single-cell RNA sequencing has been previously published.[17] All datasets are available from the corresponding author upon request.